symmetry

MDPI

Article

An Improved Near-field Magnetic Probe Radiation Profile Boundaries Assessment for Optimal Radiated Susceptibility Pre-Mapping

Audrius Merfeldas, Pranas Kuzas, Darius Gailius, Zilvinas Nakutis, Mindaugas Knyva, Algimantas Valinevicius, Darius Andriukaitis *, Mindaugas Zilys and Dangirutis Navikas

Department of Electronics Engineering, Kaunas University of Technology, Studentu St. 50-438, LT-51368 Kaunas, Lithuania; audrius.merfeldas@ktu.lt (A.M.); pranas.kuzas@ktu.lt (P.K.); darius.gailius@ktu.lt (D.G.); zilvinas.nakutis@ktu.lt (Z.N.); mindaugas.knyva@ktu.lt (M.K.); algimantas.valinevicius@ktu.lt (A.V.); mindaugas.zilys@ktu.lt (M.Z.); dangirutis.navikas@ktu.lt (D.N.)

* Correspondence: darius.andriukaitis@ktu.lt

Received: 8 June 2020; Accepted: 24 June 2020; Published: 28 June 2020

Abstract: In this paper, the near-field radiated susceptibility pre-mapping method is proposed using the improved near-field probe power radiation profile assessment. The modelling of the electromagnetic field strength in 80–3000 MHz range in the proximity of the near-field probe was performed. The −6 dB aperture boundaries of the near-field probe and their variation, due to the proximity of the radio frequency (RF) printed circuit board (PCB) components, were determined, while the aperture map distortion, arising from the proximity of the passive RF PCB components were evaluated. The scanning path requirements for the RF susceptibility mapping were determined. The simulation of improved near-field probe absolute magnetic field strength reference map in open-air conditions is carried out in this work. The comparative analysis using the absolute maximum difference metric of orthogonal absolute magnetic field map cross-sections between the reference map and magnetic field maps affected by the proximity of the components was carried out. The experimental study of the RF amplifier stage susceptibility map with susceptibility mapping measurement results are presented in this work.

Keywords: electromagnetic compatibility; electromagnetic fields; electromagnetic interference; radio frequency interference

1. Introduction

In modern smart and intelligent electronic systems, the electronic devices are exposed to broad spectrum of electromagnetic interferences. In the initial design stages of the electronic devices, the proper solutions for solving the electromagnetic compatibility (EMC) issues are crucial for compliance to the existing standards [1]. The existing testing methods for the EMC however are not able to spot the susceptible areas of the printed circuit boards (PCBs) and the Pass/Fail report format does not give a detailed insight or the reference for developers of the PCB layout. A variety of the applications and recent research, including the EMC characterization of electrical machines [2], smart power grid devices [3], near-field emissions of mobile devices [4], industrial robotics [5], automotive equipment [6], military and avionics [7] are based on the electromagnetic (EM) field emission mapping method, using the electric or magnetic field (MF) [8] receiving probes [4]. The method is able to point the areas with increased EM field emission of the scanned area. However, for more comprehensive characterization of the electronic device solution, the radiated susceptibility mapping has certain advantages, since it is possible to spot the susceptible areas of RF boards where board signal levels are insufficient for effective

assessment of the radiated emissions such as RF input stages, shielding, DC power circuitry, ground connections, high speed lines [9], open loops, or PCB traces [10], etc. where external disturbances may degrade the performance of a given stage or device in its entirety. The radiated susceptibility mapping resolution improvement and error reducing [11] are achieved, either by improvement of the probe design [12], or by post processing the acquired map data [13]. The electric and magnetic near-field probes for radiated susceptibility mapping exist. However, the magnetic probes are less prone to the proximity of the PCB ground plane and protruding components. The microstrip near-field magnetic probe performance investigated by the authors [12] yielded to 22–47% improved radiated susceptibility mapping resolution in the 80–3000 MHz range in the proximity of the coplanar waveguide. Due to the PCB landscape and variation of component height, density and magnetic properties, not all areas can be scanned in close proximity, and therefore, the resolution and accuracy of the radiated susceptibility map degrades. The adaptive scenario of the prescanning and successive field susceptibility scanning is beneficial in the suspicious areas of the device under test. The coupling efficiency variations and the probe aperture variations, due to the variable scanning height should be encountered in the pre-scanning stage with the purpose to equalize the injected MF strength at the PCB board level over the frequency range. Based on the previous research and experience gained by authors [12] in the electromagnetic compatibility field, the adjustable scenario of radiated susceptibility mapping can benefit both from structural improvement of the probe and characterization of its performance under scanning conditions. Hardware adjustments at some degree in the probe RF power stage, such as equalization of the probe frequency response curve or gaining control can be performed, in order to reduce the variation of the coupling coefficient. The probe compensation methods [11] or susceptibility map post-processing techniques may be combined for adjustment of the acquired data, and therefore, improve the map resolution. In the radiated susceptibility mapping, it is important to determine the spatial resolution over the frequency range, and to optimize the scanning time and amount of the scanning points. Another important aspect of the radiated susceptibility mapping is to maintain the injected MF strength at the surface of the board within the predetermined levels relevant to the existing standards. Since the PCB components are present in the proximity of the probe, their influence research to the MF strength distribution and to the aperture shape of the improved probe is considered worthwhile by authors. Therefore, the aim of this work is to model the near-field magnetic probe aperture for the improved probe, proposed by authors, and to determine the influence of the PCB structure and component proximity to the performance of the probe in the 80–3000 MHz frequency range. More specifically, the probe aperture map, its distortions and spatial resolution will be assessed by means of simulation, and the susceptibility pre-mapping measurement results will be presented in this work. The recommendations for the near-field probe MF map distortion assessment will be given. The paper is organized as follows. In the Chapter 3, the model of the near-field magnetic probe and the simulated near-field MF strength in open-air conditions of the probe are presented. The reference MF aperture map is defined and the detailed models of the passive components are given. Chapter 4 is dedicated to the simulation of the MF map distortions due to the presence of the passive components in the proximity of the improved probe. The experimental application of the probe is demonstrated in in the Chapter 5. Pre-scanning and detailed scanning results of the radiated susceptibility map are presented, followed by discussion and conclusions. The list of abbreviations provided in Appendix A, Table A1.

2. Methodology

Aiming to determine the EM field distribution and aperture shaping parameters of the MF probe in the near-field zone, the improved MF probe [12] was modeled in the CST Studio Suite environment. The modeling is performed in four stages: (1) the EM field distribution of the MF probe is modeled in open air without PCB board or other components in the proximity of the probe; (2) the aperture of the near-field probe was simulated in the proximity of the PCB board with 50 Ω impedance microstrip line; (3) the simulation is performed with presence of different types of surface mounted components

(SMD) located at 5 mm distance from the probe on the disrupted microstrip line. The EM field strength distribution was estimated in the 80–3000 MHz frequency range; (4) the MF absolute strength map for prescanning of the PCB board is composed and the measurement results are acquired using the improved probe. The geometry of the improved near-field probe, modelling conditions and simulated probe apertures are elaborated in Chapter 3.

3. Probe Magnetic Field Characterization in Open-Air Conditions

3.1. Geometry of the Probe

The improved near-field magnetic probe model geometry developed in the CST Studio Suite software for estimation of near-field EM distribution is presented in the Figure 1. The RF power is connected to the probe input 50 Ω port 1. The probe is encapsulated in the copper cylinder 2 with internal diameter of 8 mm for improved focusing of the MF. The probe is produced using the microstrip technology on the FR-4 laminate 4. The tapered line 3 is used for the improvement of the broadband matching of the magnetic loop 6 which is shaped as a rectangular trace loop on the top layer of the probe PCB with parameters d = 5.3 mm and w = 0.3 mm. The loop feed is provided through the PCB via 5 to the ground polygon of the bottom layer (Figure 1b).

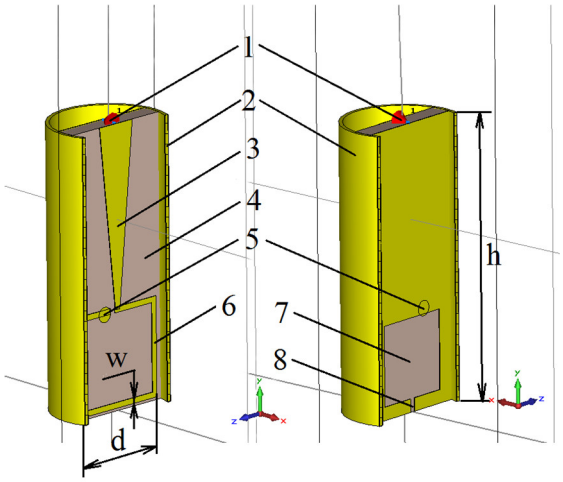

Figure 1. Near-field magnetic probe model geometry in the CST Studio Suite.

The 5 × 5 mm copper area is removed from the ground layer and the 0.3 mm gap 8 for the high frequency (HF) current path management is formed near the working edge of the probe PCB. The probe construction allows for close proximity to the PCB under the test, as the copper cylinder and working edge are aligned.

3.2. Modelling of the Near-Field Probe

The near-field probe model is presented in Figure 2. The criteria of 30 grid elements per minimal wavelength was set while generating the mesh grid for the 3D (three-dimensional) model time domain solver in the CST Studio Suite. The cell dimension range was from 0.0175 mm to 3.29 mm; total number of 3,143,448 adaptive hexahedral mesh elements was generated in the solver for simulation. The EM field calculation results in the model by default are acquired in the 3D field monitors as a color map at a chosen frequency. For numerical data exporting purposes, the grid consisting of 169 isotropic EM field virtual probes in the proximity of the magnetic near-field probe were displaced in the *XZ* plane of the model (see Figure 2). The virtual probe grid density is 1 mm. A 101 × 2 element length array of absolute MF strength values versus frequency (80–3000 MHz range) is exported to the data file. The

distance from the probe grid plane in the model was set in the range from 3 mm to 15 mm to cover the most probable range of distances for pre-scanning purposes.

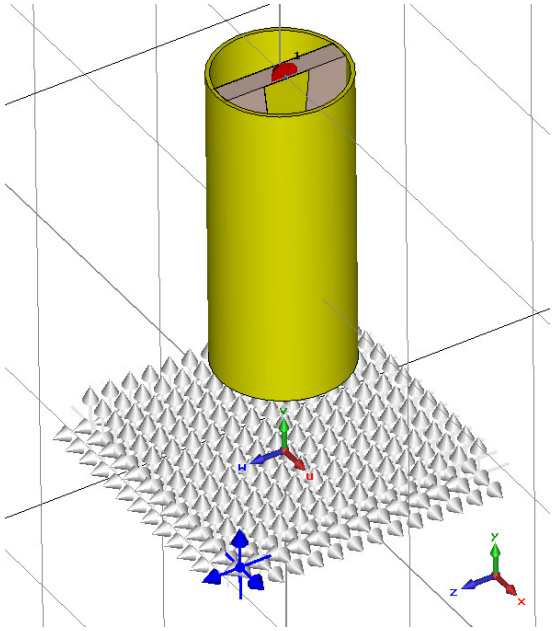

Figure 2. Near-field magnetic probe model in the CST Studio Suite.

The −6 dB relative MF decrease margin regarding the peak value at the center of the near-field probe is used to define the aperture of the probe. For the first stage, the open-air conditions were created and the simulation was performed at 3, 5 and 10 mm distance. The simulation results at 1000 MHz probe excitation frequency are shown in Figure 3. The contour of the copper cylinder was highlighted as red color ring and isolines of the MF strength in 0.2 dB increments were overlaid to display the distribution of the MF in the XZ plane. The offset of the MF distribution and therefore the probe aperture shift is observed in the proximity of 3 mm (see Figure 3a). The elliptic shape of the −6 dB aperture is evident in bigger distances at 5 mm and 10 mm (see Figure 3b,c).

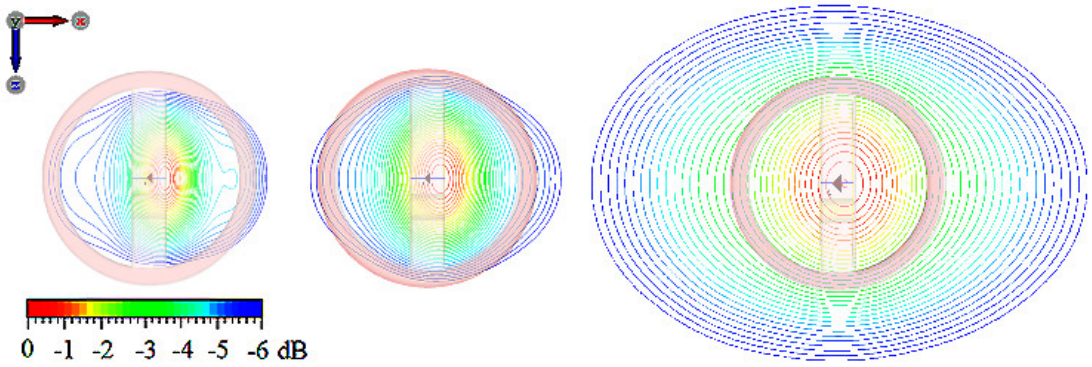

Figure 3. Near-field magnetic probe relative MF strength −6 dB apertures in the CST Studio Suite: (**a**) 3 mm distance, (**b**) 5mm distance, (**c**) 10mm distance.

In the open air conditions, the MF strength distribution in the proximity zone of the near-field probe has single global maximum value and the cross-section of the absolute MF strength map can either be approximated with a low order polynomial or interpolated. To define the MF aperture

diameters and their variation over the frequency range, the aperture cross-sections in XY plane and ZY planes were estimated. The results are presented in Figure 4.

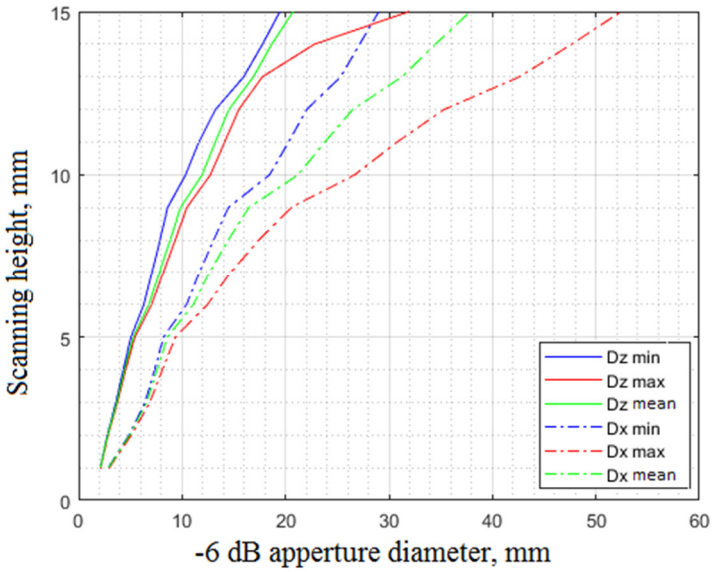

Figure 4. Modeled near-field magnetic probe averaged aperture sizes (green and green dotted lines) and min-max aperture size boundaries over 80–3000 MHz range.

Interpolated apertures in the 80–3000 MHz range were simulated and their average values in the given frequency range are displayed in the Figure 4 by the green line (ZY plane) and green dotted line (XY plane). The maximum (red and red dotted lines) and minimum (blue and blue dotted lines) aperture measures were determined respectively. The maximum and minimum measures represent the worst case limits of the modeled aperture size through the analyzed frequency range. The performance of the near-field probe can be defined by two parameters:

1. The slope of average −6 dB aperture diameter over the scanning distance in the given plane $D\text{-}_{6dB}(H)$
2. Variance of the probe aperture over the given frequency range $\sigma_{-6dB}(H)$

It may be noted from the Figure 4, that in the ZY plane, the value of the $D_{-6dB}(H)$ slope is higher than that in the XY plane. Yet, the variance of the $D_{-6dB}(H)$ slope in the ZY plane is also smaller, which indicates improved focus on the injected MF and the better susceptibility mapping resolution in the ZY plane. A trade-off between the near-field probe aperture dimensions and the scanning height above the PCB must be considered for precise locations of the hotspots in radiated susceptibility maps. For pre-scanning, maximizing the scanning speed at a constant scanning height with a predefined injected absolute MF strength and predictable injected MF strength variation limits are preferred. The mid-range of pre-scanning at 5 mm height above the PCB was chosen for more detailed analysis. It can be seen in Figure 4 that the probe aperture size boundaries' variation in the 80–3000 MHz scanning frequency range at open air conditions is less than 20% both in ZY and XY planes at 5 mm scanning height. The effective scanning height in the ZY plane therefore is higher than that in XY plane and reaches up to 8 mm for 20% aperture size variation boundary. The MF strength map display form as a 3D mesh grid surface is used in the following sections for analysis. Due to the numerous degrees of freedom, modelling results will be presented in case of fixed scanning height. The full definition of geometric parameters of the model is presented in the Table 1.

Table 1. Probe model geometry definition.

Probe Model Geometry Parameter	Parameter Value
Microstrip line impedance	50 Ω
Microstrip PCB dimensions	100 × 20 mm
Base laminate thickness	1.5 mm
Base laminate Dk	4.2
Distance from probe working edge to the microstrip top layer surface	5 mm
Virtual absolute MF probes' grid density	1 × 1 mm
Virtual absolute MF probes' quantity	169
Virtual absolute MF probes' coverage area	13 × 13 mm
Virtual absolute MF probe grid depth below the surface of the microstrip top layer	0.1 mm
Probe RF port excitation power level	27 dBm

3.3. Modelling of the Near-Field Probe MF Strength Distribution Map in Open-Air Conditions

The absolute MF strength distribution in the proximity zone of the probe and its variation due to the changing conditions of scanning may be handled in the radiated susceptibility map post-processing algorithms. The exported data from the isotropic EM field virtual probe map (see Figure 2) is used for estimation of the MF distribution. The open-air modelling results at 1000 MHz frequency are presented in Figure 5. It can be seen from the magnetic probe aperture map in Figure 5 that variation of the MF strength is within 16 dB in the 13 × 13 mm modeled area.

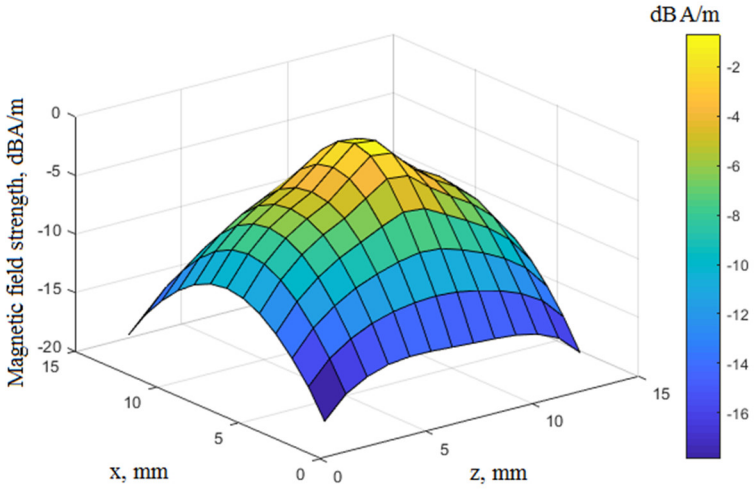

Figure 5. Modeled near-field magnetic probe aperture map sample in XZ plane at 1000 MHz at 5 mm distance.

The resulting near-field magnetic probe aperture shape at the open-air condition will be used as a reference for comparison of the apertures in case of other conditions (probe loads). The open-air map with a ninth order two-dimensional (2D) polynomial approximation over 80–3000 MHz frequency range is shown in Figure 6. The approximation metrics are R^2 = 0.9990, RMS error (RMSE) = 0.1324, DoF = 114. The polynome expression is presented in the previous research provided by the authors [14].

In high frequency applications, the probe is in the proximity of the PCB surface and surface mounted components which have magnetic materials in their construction. Due to the proximity of conductive elements, a part of the MF energy would be absorbed and transferred to the PCB as the injected field. Another part of energy is deflected or reflected by the component presence or displacement, and thus, distorting the apparent magnetic probe aperture. The according modelling will be performed and discussed in more detail in the next section.

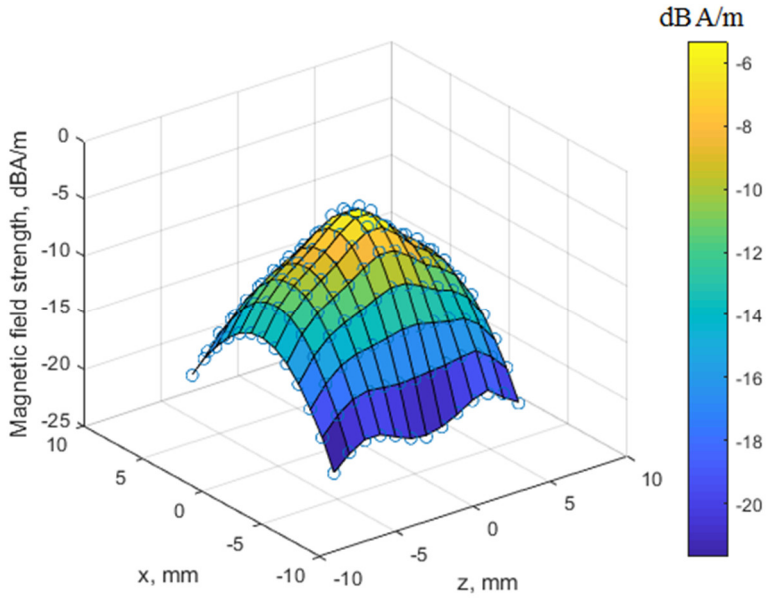

Figure 6. Modeled near-field magnetic probe aperture map in XZ plane averaged over 80–3000 MHz frequency range at 5 mm distance approximated by ninth order polynome.

4. Modelling of the Near-Field Probe Magnetic Field Strength Distribution in Proximity to the Passive Components

Using the models developed in Chapter 2 of this paper, the simulation of absolute MF strength was performed. The results in the form of 3D mesh grid will be presented and the cross-sections in XY and ZY planes of the absolute MF map will be used for comparison both for aperture and for MF distortions. The samples of MF maps will be presented at 1000 MHz frequency. For the comparison with a reference averaged absolute MF strength map in open-air conditions developed in Chapter 2 Section B, metrics in the form of maximum MF strength absolute difference will be applied for three characteristic frequency points (80 MHz, 1000 MHz and 3000 MHz).

4.1. Characteriztion of the Passive Components in the Proximity of the Near-Field Probe

Some of the RF solutions that are subject and cause of the radiated susceptibility mapping hotspots are the PCB traces and polygons which may form RF filters, couplers, transmission lines, ground planes and vias. They do not exhibit magnetic properties when plated with solder paste or covered by a solder mask. The distortion of the near-field magnetic probe aperture correction map may appear due to local trace coupling, losses and reflections of the injected MF in the tracks and ground loops. Another group of objects is a variety of components which are used in the RF PCB boards including integrated circuits (IC) chips, resistors, capacitors, inductors, transformers, holders, etc. These components contain magnetic materials in their leads or in the body and therefore they tend to distort the MF injected by the probe. In this section, the distortion of MF distribution and influence to the near-field probe aperture geometry will be carried out. The simulation of microstrip line and three types of objects soldered on the microstrip line gap (resistor, capacitor and chip inductor, all of them of 0805 form factor) was performed. The model of the near-field probe at 5 mm distance for the microstrip line is shown in Figure 7.

The microstrip line was implemented as a 50 Ω impedance trace formed on the top layer of the FR-4 laminate. Both input and output of the line were terminated with a broadband matched ports. The virtual array of absolute MF probes was positioned below the surface of the top copper layer in the model. The MF strength in the 0.1 mm depth under the copper trace of the microstrip line was measured. The displacement of the grid and the highlighted generalized component geometry are presented in Figure 8.

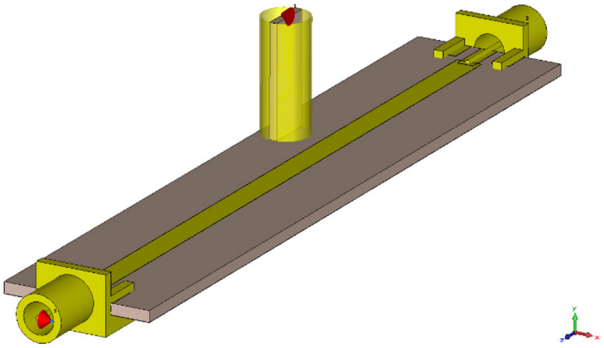

Figure 7. Near-field magnetic probe in 5 mm proximity from the microstrip line trace.

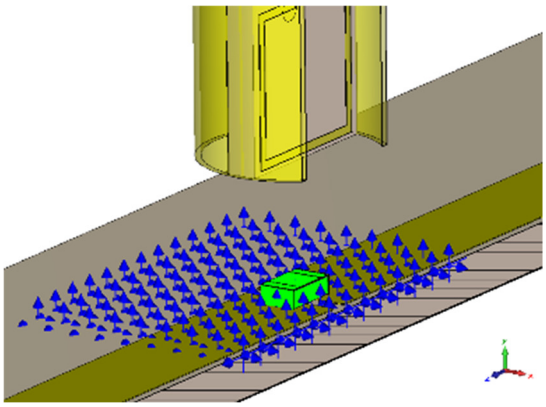

Figure 8. Near-field magnetic probe in 5 mm proximity from the microstrip line trace with a generalized component geometry on the microstrip gap.

For discovering of specific signatures in the magnetic probe aperture map induced by presence of the passive components, detailed models of these components were created. The 0805 element form factor was chosen for the model size. The material composition and internal layer distribution of the components was acquired from the user manual component specifications and technical spreadsheets provided by manufacturers TDK, Wurth and Murata. The geometry of the resistive component is presented in Figure 9.

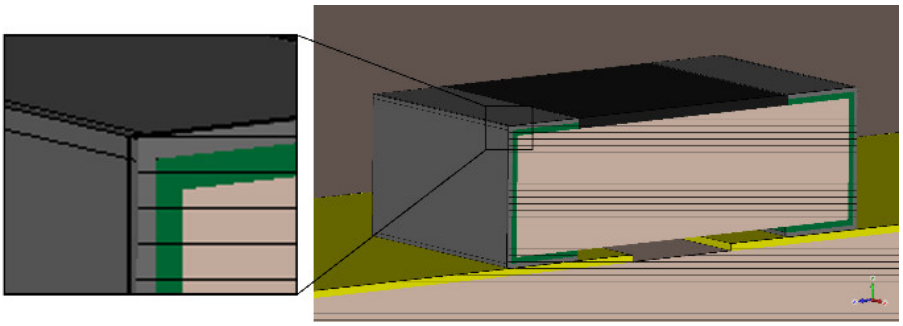

Figure 9. Resistive component model cross-section for MF attenuation and probe aperture map distortion estimation.

The resistive component of 1 kΩ was created in the CST Studio Suite environment. The base of the model is ceramic Al_2O_3. Resistive carbon layer with thickness of 0.02 mm was used as film with the protective coating layer of glass. The conductive leads of the component are formed from internal nickel (Ni) and external tin (Sn) layers. The full specification of the resistor model geometry and material composition is given in the Table 2.

Table 2. Resistor model parameters.

Resistor Model Parameter	Parameter Value
Base dimensions	2 × 1.25 × 0.6 mm
Protective coating thickness	50 µm
Resistive layer thickness	20 µm
Internal contact material	Ni
External contact material	Sn
Resistive layer material	RuO_2
External electrode grip length	420 µm
Internal electrode metallization thickness	30 µm
External electrode metallization thickness	20 µm

Multilayer capacitor model was developed for the simulation of the MF. The cross-section of the model is presented in Figure 10.

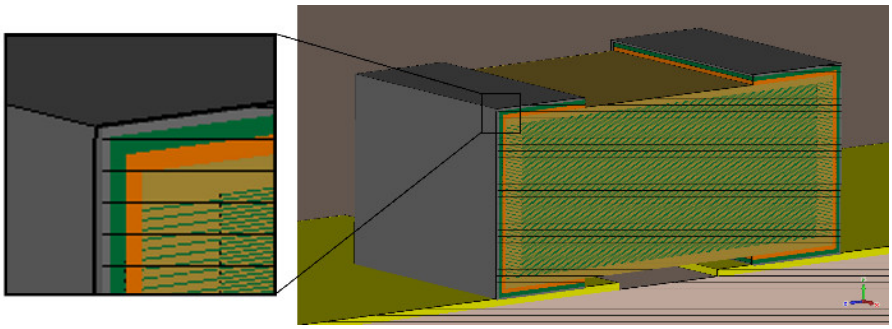

Figure 10. Capacitive component model cross-section for MF attenuation and probe aperture distortion estimation.

A XR7 base ceramic material with 150 pairs of nickel and copper plates was used. Full specification of the capacitor model is presented in Table 3.

Table 3. Capacitor model parameters.

Capacitor Model Parameter	Parameter Value
Base dimensions	2 × 1.25 × 0.8 mm
Base material	$BaTiO_3$ X7R
Internal capacitor plate material	Ni
Internal contact material	Cu
Middle contact material	Ni
External contact material	Sn
Number of capacitor electrode pairs	150
Capacitor plate metallization thickness	2 µm
Distance between capacitor plates	3 µm
Percentage of capacitor plates overlap	95%
External electrode grip	530 µm

The horizontal winding type inductive component chip ferrite bead model was developed for simulation of the MF. The cross-section of the model is presented in Figure 11.

The detailed specification of the horizontal winding type for RF chip ferrite bead model is presented in Table 4.

The simulation results using the models described above, of the absolute magnetic field strength distribution under the PCB microstrip line will be presented in the following chapter.

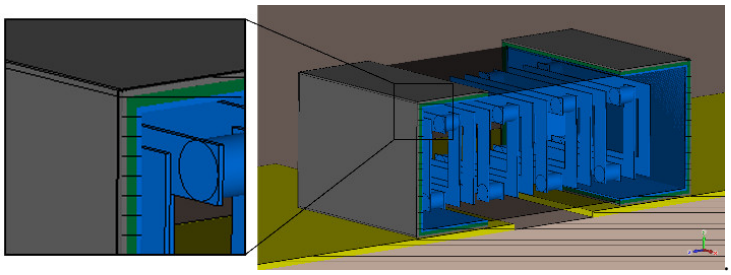

Figure 11. Inductive component chip ferrite bead model for magnetic field attenuation and probe aperture distortion estimation.

Table 4. Inductor model parameters.

Inductor Model Parameter	Parameter Value
Ferrite base dimensions	1.9 × 1.1 × 0.75 mm
Ferrite material	NiZn
Internal electrode material	Ag
Middle electrode material	Ni
External electrode material	Sn
Number of turns	16
Orientation of windings	Horizontal
Winding loop width	900 µm
Winding loop height	550 µm
Winding wire thickness	10 µm
Winding wire width	100 µm
Inter-winding distance	120 µm
Diameter of inter-winding vias	100 µm
Internal electrode metallization thickness	10 µm
Middle electrode metallization thickness	10 µm
External electrode metallization thickness	10 µm
External electrode grip length	500 µm

4.2. Absolute Magnetic Field Distribution Map Modelling

The absolute MF distribution map at 1000 MHz in the 5 mm proximity from the microstrip line model developed in Section 4.1 see Figure 7) is shown in Figure 12. A distortion of the MF map in a shape relevant to the geometry of microstrip line trace is visible at 1000 MHz frequency. The shielding and MF coupling effects into the microstrip line contribute to the resulting map shape.

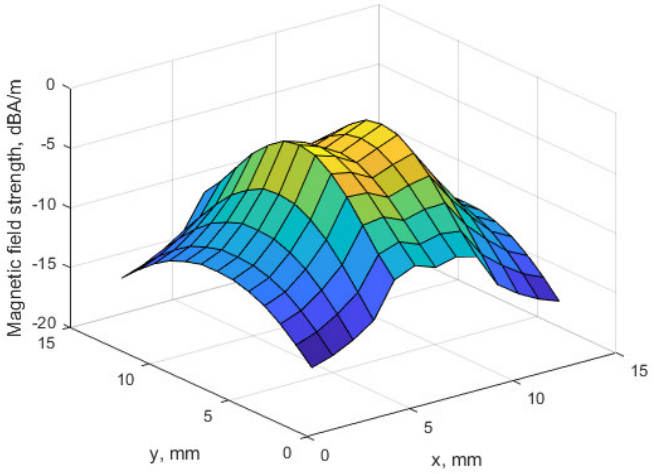

Figure 12. Near-field magnetic probe aperture map in XZ plane in 5 mm proximity from a microstrip line at 1000 MHz.

In the case of a 1 kΩ resistor displaced on the microstrip line abrupted trace, the MF map is presented in Figure 13. Lower coupling efficiency and therefore higher MF strength at the center of the component is observed.

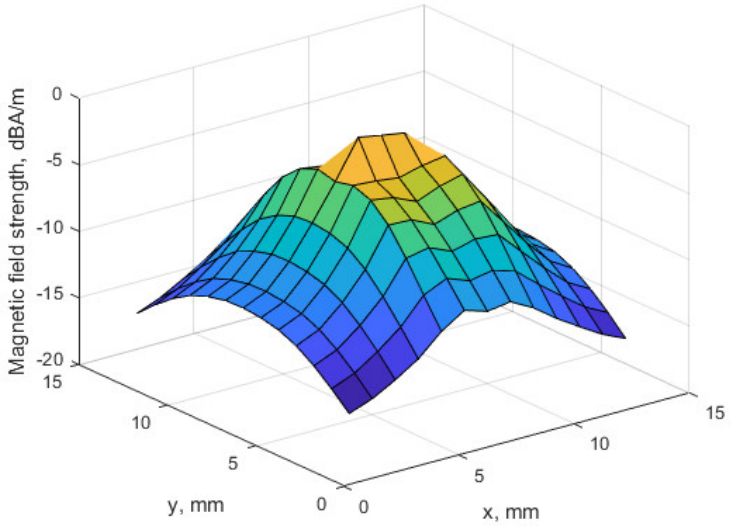

Figure 13. Near-field magnetic probe in the proximity of a microstrip trace with a resistor at 1000 MHz.

A similar behavior is noticeable in the case of multilayer capacitor model (see Figure 14). The MF map protrusion at the center of capacitor body reaches −0.5 dBA/m at 1000 MHz.

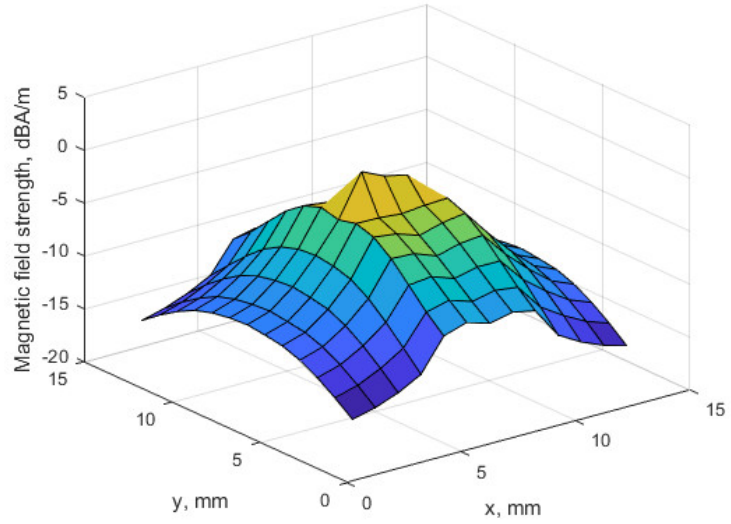

Figure 14. Near-field magnetic probe in the proximity of a microstrip trace with a capacitor at 1000 MHz.

The chip ferrite bead absolute MF distribution map at 1000 MHz is shown in Figure 15. The characteristic double top signature is observed in the results due to the magnetic coil secondary MF interaction with the injected field.

For comparative analysis of the absolute MF map distortion due to the proximity of the modeled microstrip line and passive components, the cross-sections in XY and ZY planes of the mesh grids (Figures 12–15) were analyzed. The average approximated open-air map developed in Section 3.3 (Figure 6) was used as a reference. The resulting modeled cross-sections of four types of proximity components at 1000 MHz frequency are shown in Figures 16 and 17.

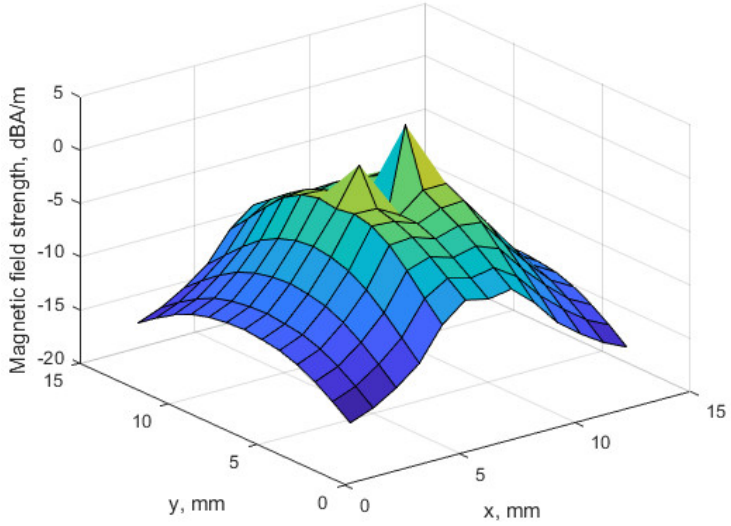

Figure 15. Near-field magnetic probe in the proximity of a microstrip trace with a ferrite bead at 1000 MHz.

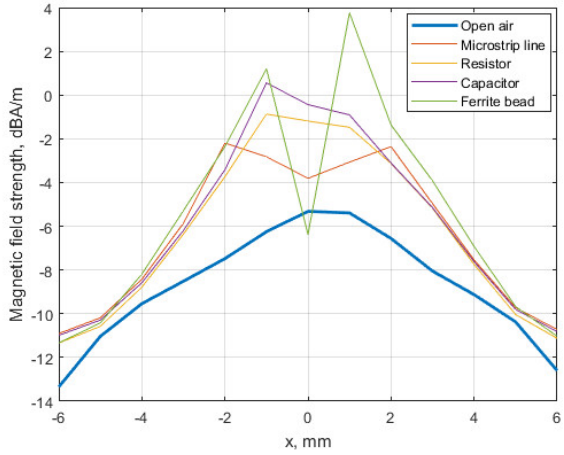

Figure 16. MF map cross-section in XY plane at 1000 MHz.

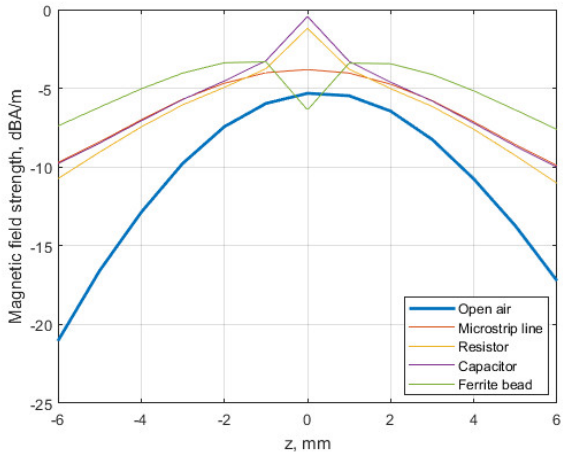

Figure 17. MF map cross-section in ZY plane at 1000 MHz.

The maximum absolute difference metric between the reference map in open-air conditions and each component at three characteristic frequencies was applied for the modelling results. The comparison of the MF strength at 0.1 mm depth under the PCB surface and MF strength variation boundaries is given. The results are presented in Table 5.

Table 5. Absolute magnetic field distortion.

Type	Max Absolute Differences from Open Air, dB					
	80 MHz		1000 MHz		3000 MHz	
	XY	ZY	XY	ZY	XY	ZY
Microstrip line	7.95	11.37	5.28	11.32	13.38	14.89
Resistor	8.90	13.49	5.38	10.30	2.40	11.84
Capacitor	8.65	11.46	6.81	11.25	9.86	16.58
Ferrite bead	12.22	15.92	9.15	13.65	10.46	13.71

From the simulation results in this section, it may be pointed that the MF strength distribution in the proximity of the microstrip line exhibits the absolute MF strength attenuation, which displays both flattening and distortion effects of the magnetic probe aperture. In the 1000 MHz MF map cross-section, the distortion effect is present in the central area which covers ±2 mm and can be considered as local. The local distortion of the absolute MF map is observable in XY and in ZY planes. The flattening effect has a larger influence to the selectivity performance of the improved MF probe. From the absolute difference metric results given in the Table 5 it can be noted that the flattening effect is more evident in the ZY plane and this tendency remains over all frequency range.

The trade-off between scanning resolution and scanning speed should be considered for each radiated susceptibility map. For pre-scanning purposes, the scanning speed is considered as the deciding factor. The density of the scanning points in the RF PCB pre-scanning stage depends on the probe used, as well as on the scanning height and aperture size. Considering the simulation results of the generalized aperture and MF distribution in the proximity of the improved near-field probe, the pre-scanning task was formed. The following considerations were taken into account: (a) The minimum aperture overlapping should be achieved to decrease the scanning grid density; (b) the strategy of minimum moving path should be applied to increase the moving speed between the scanning points. The scanning grid can be characterized by steps s_x and s_y:

$$s_x(h) = \frac{3 \cdot r_{ax}(h)}{2 \cdot \sqrt{3}}, \tag{1}$$

$$s_y(h) = 1,5 \cdot r_{ay}(h), \tag{2}$$

where $s_x(h)$ is scanning step in x direction, $s_y(h)$ is scanning step in y direction, h is scanning height, $r_{ax}(h)$ is −6 dB aperture radius along the x axis, $r_{ay}(h)$ is −6 dB aperture radius along the y axis.

The probe aperture diameter was approximated by a circle using the maximum 5.3 mm diameter of the −6 dB probe aperture. The radiated susceptibility map scanning path strategy is shown in Figure 18.

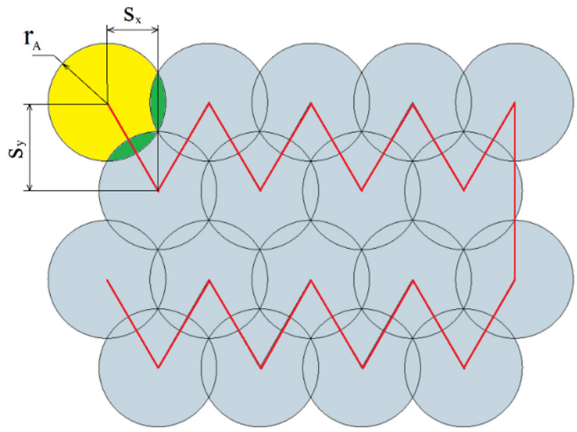

Figure 18. Radiated susceptibility map scanning strategy.

From the results presented in Figure 18, the absolute MF strength map at the surface of the PCB under the test with corrections applied according to the Table 5, can be used for the generation of the effective radiated field with minimum overlap criteria at −6 dB margin. The grid representation suitable for prescanning purposes was proposed and the map is shown in Figure 19.

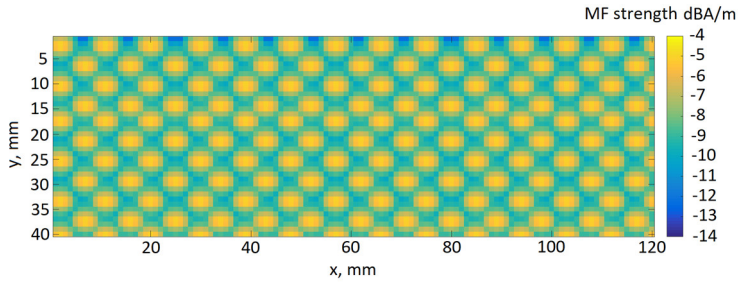

Figure 19. Effective radiated MF simulated in open-air conditions for prescanning of the PCB under the test.

The scanning results using measurement system and the criteria and assumptions formulated in Chapter 3 will be used in the next chapter.

5. Experimental Probe Verification

5.1. Measurement System Setup

The radiated susceptibility mapping experimental system was designed for pre-scanning and scanning of the PCB under the test. The structure of the system is presented in the Figure 20 and it consists from the xyz scanner stage 1 equipped with linear bar guides with linear bearings, feed screws with reduced backlash and stepper motors driven by the microcontroller with the GRBL image for G-code compatibility 5 with micro-stepping, simultaneous x and y axis displacement and motion acceleration/deceleration functionality.

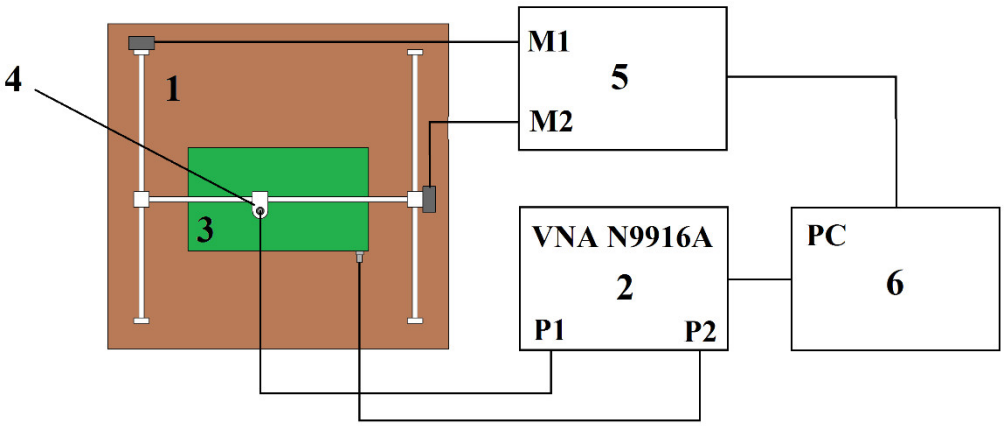

Figure 20. Radiated susceptibility mapping experimental system. 1—xyz scanner, 2—VNA FieldFox N9916A, 3—device under test, 4—magnetic near-field probe, 5—stepper motor controller, 6—computer.

The scanning path of the xyz scanner stage is controlled through G code commands by the computer 6. The probe excitation is performed and coupling is measured by the handheld VNA FieldFox N9916A 2. The device under the test 3 is placed on the scanning area and the probe 4 height is set to 5 mm above the PCB. The scanning process and data acquisition from the VNA is controlled by the software implemented in the Matlab environment.

The RF amplifier stage with a gain block with power filter circuitry and 50 Ω traces was utilized for scanning. The PCB board dimensions were 100 by 20 mm.

5.2. Prescanning and Scanning Results of the Radiated Susceptibility Map

The pre-scanning of the radiated susceptibility map was performed using the improved MF probe. 203 scanning points were used for prescan. The scanning path strategy defined in the Section 2 of Chapter 4 was applied. The pre-scan resolution was set to 5.3 mm both in x and y axis.

Using the prescanned magnetic near-field susceptibility map, presented in Figure 21, the susceptible areas of the PCB under the test are detectable. As it may be identified from the pre-scan results, the sensitive areas correspond to the input feedline and input of the RF amplifier as well as the output connector.

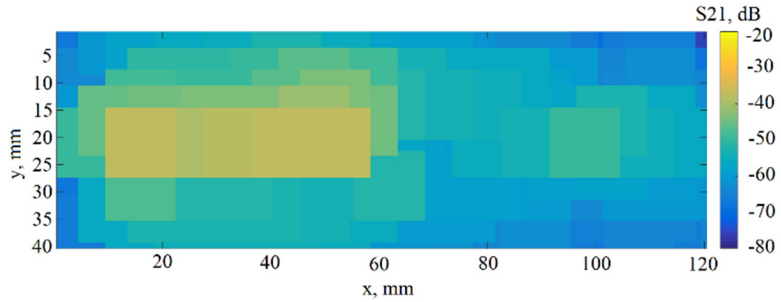

Figure 21. Magnetic near-field susceptibility pre-scan map at 5.3 mm scanning resolution at 1000 MHz.

Detailed magnetic probe aperture mapping result is shown on Figure 22. The detailed map with 1 mm resolution approved the problematic areas identified in the prescanning stage. The improved scanning resolution is allowed to visualize and localize the susceptible areas.

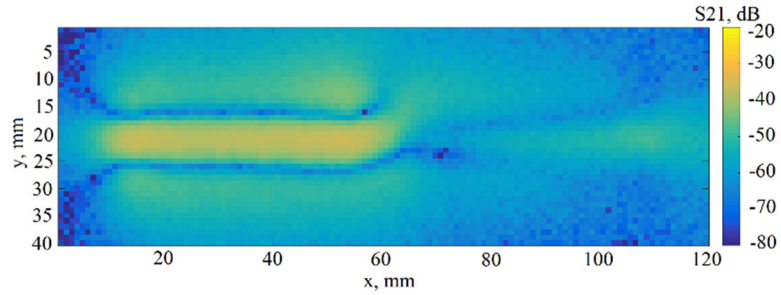

Figure 22. Magnetic near-field susceptibility map at 1 mm scanning resolution at 1000 MHz.

The pre-scan procedure took up 4 min. and 30 sec. The full scan duration was 20 min. and 5 sec. For better trade-off between scanning time and radiated susceptibility map resolution, the scanning of PCBs with high complexity RF nodes are subject of adaptive scanning, which is foreseen in a future research of the magnetic field radiated susceptibility mapping post processing and optimization.

6. Discussion

The results of MF absolute strength simulations in the proximity of the PCB improved probe allow for the estimation and corrections of the MF distribution across the aperture. The method accounts generalized aperture distortions using absolute field strength absolute difference as a measure. The scanning of the board using a generalized absolute MF strength correction in the post-processing stage was performed and the radiated susceptibility map was obtained. The efficient hotspot localization can be performed at the 80–3000 MHz frequency range and beyond. The attenuation ratio due to shielding and absorption in the top layer of the microstrip line was determined and in the proximity of the PCB, the dual effect is noticeable. Firstly, the MF energy is partially reflected due to the presence of the ground plane and secondly, the coupling efficiency variation over the frequency range due to the mutual relation of wavelength and dimensions of the hotspot. The latter effect dominates in low

frequencies. Assumptions for equalization of the absolute MF strength in different PCB layers were drawn and they can be used for post-processing of the radiated susceptibility map. For more detailed specification of the improved magnetic probe, the vectors of the MF and their distortion could give a better insight and more accurate prediction of the injected MF variations for different areas of the board, which is a subject of future research.

7. Conclusions

The results of MF absolute strength simulations in the proximity of the PCB improved probe were analyzed. Five cases of the proximity components were modeled, including open-air, microstrip line and three passive components. The reference MF aperture in the open-air conditions was defined and approximated by the ninth order polynomial. Due to the presence of the passive components, the characteristic local MF distortions in the ±2 mm area of the improved magnetic probe axis were determined. The local distortion of the MF aperture is within 10 dB at 1000 MHz. From the obtained results, the pre-scanning conditions were drawn by defining the population of components on the board under the test. The boundaries of variance determined by the maximum absolute difference metric between the reference map cross-sections in open-air conditions and corresponding cross-sections of the distorted maps (Table 5), allowed to assess the probable fluctuations of the absolute MF strength in deeper layers of the PCB board. The practical confirmation of simulated results is not possible due to the small scanning distances, physical dimensions of the real probe and probe influence to the field. The MF map distortion data could contribute to the selection, detection and classification of the PCB hotspots for automated adaptive pre-scanning and scanning tasks.

Author Contributions: Conceptualization, A.M., P.K., D.G., D.A. and D.N.; methodology, A.M., A.V. and M.Z.; software, M.K. and D.N.; validation, P.K., Z.N. and M.Z.; formal analysis, P.K., Z.N., M.K. and A.V.; visualization, D.G., Z.N., D.A. and D.N.; investigation, A.M., A.V. and D.A.; resources, M.K., D.A. and M.Z.; data curation, A.M., M.K. and M.Z.; writing—original draft preparation, A.M., P.K., Z.N. and M.K.; writing—review and editing, P.K., D.G., Z.N., A.V. and D.N.; Supervision, D.G. and D.A.; funding acquisition, D.G., A.V., M.Z., and D.N. All authors have read and agreed to the published version of the manuscript.

Funding: This research received no external funding.

Conflicts of Interest: The authors declare no conflict of interest.

Appendix A

Table A1. List of abbreviations.

Abbreviation	Definition
DC	Direct Current
EM	Electromagnetic
EMC	Electromagnetic Compatibility
HF	High Frequency
IC	Integrated Circuit
MF	Magnetic Field
PCB	Printed Circuit Board
RF	Radio Frequency
SMD	Surface Mount Device
VNA	Vector Network Analyzer

References

1. Electromagnetic Compatibility (EMC) International Standard IEC 61000-4-20: "Testing and Measurement Techniques—Emission and Immunity Testing in Transverse Electromagnetic (TEM) Waveguides", IEC. 2003. Available online: https://webstore.iec.ch/publication/4190 (accessed on 8 June 2020).
2. Brahim, S.B.; Bouallegue, R.; David, J.; Vuong, T.H. Study and improvement in the radio communication quality for rotating electrical machine. *Electr. Eng.* **2019**, *101*, 855–865. [CrossRef]

3. Lukočius, R.; Nakutis, Ž.; Daunoras, V.; Deltuva, R.; Kuzas, P.; Račkienė, R. An Analysis of the Systematic Error of a Remote Method for a Wattmeter Adjustment Gain Estimation in Smart Grids. *Energies* **2018**, *12*, 37. [CrossRef]
4. Lee, S.Y.; Kim, Y.J.; Kim, J.J.; Kim, J.M.; Yang, K.M. Methodology for RF receiver sensitivity analysis using electromagnetic field map. *Electron. Lett.* **2014**, *50*, 1753–1755.
5. Łukasik, Z.; Kuśmińska-Fijałkowska, A.; Kozyra, J.; Putynkowski, G.; Woźny, K. The problem of power supply for station with industrial robot in an automated welding process. *Electr. Eng.* **2018**, *100*, 1365–1377. [CrossRef]
6. Liu, G.; Zhong, S. Research on an Electromagnetic Interference Test Method Based on Fast Fourier Transform and Dot Frequency Scanning for New Energy Vehicles under Dynamic Conditions. *Symmetry* **2019**, *11*, 1092. [CrossRef]
7. Baqar, A.H.; Jiang, T.; Hussain, I.; Farid, G. Probability of Conjunction Estimation for Analyzing the Electromagnetic Environment Based on a Space Object Conjunction Methodology. *Symmetry* **2018**, *10*, 255. [CrossRef]
8. Alves, H.; Carvalho, D.; Pereira, T.; Fernandes, H. Design and instrumentation of a magnetic field micro-probe mapper: An e-lab aparatus to map a coil's magnetic field. In Proceedings of the 2017 4th Experiment International Conference, Faro, Portugal, 6–8 June 2017; pp. 113–114.
9. Byun, J.; Lee, H. Analysis and Improvement of Electromagnetic Susceptibility on High Speed LVDS I/O System. *Measurement* **2010**, 175–178. Available online: https://ieeexplore.ieee.org/abstract/document/5728619/citations#citations (accessed on 8 June 2020).
10. Merfeldas, A.; Kuzas, P.; Gailius, D.; Andriukaitis, D. Characterization of radiated susceptibility directivity for microstrip and coplanar lines. In Proceedings of the European Microwave Conference in Central Europe EuMCE, Prague, Czech Republic, 13–15 May 2019; pp. 125–128.
11. Claeys, T.; Vandenbosch, G.A.E.; Pissoort, D. A study of the effects of truncation errors on the compensation of EMI near-field probes. *IEEE Int. Symp. Electromagn. Compat.* **2016**, *11*, 23–28.
12. Merfeldas, A.; Kuzas, P.; Gailius, D.; Nakutis, Z. Magnetic probe for improvement of near-field resolution in radiated susceptibility mapping. *Electron. Lett.* **2019**, *55*, 940–942. [CrossRef]
13. Boyer, A. Improving spatial resolution of immunity maps by post-processing. *Asia-Pacific Int. Symp. Electromagn. Compat.* **2016**, *1*, 56–59.
14. Merfeldas, A.; Kuzas, P.; Gailius, D.; Nakutis, Z.; Knyva, M.; Valinevicius, A.; Andriukaitis, D.; Zilys, M.; Navikas, D. Magnetic Near-field Probe Radiation Profile Boundaries Assessment for Radiated Radio Frequency Susceptibility Mapping. *Elektro* **2020**. to be published.